Contributions to Geophysics and Geodesy Vol. 54/3, 2024 (225–250)

Delineation of subsurface features by electrical resistivity tomography and induced polarization in upstream basin of Chaq-Chaq dam – northeastern Iraq

Abdulla K. AMIN[1,*], Sazan S. MOHAMMED[2], Ezzadin N. BABAN[3]

[1] Department of Social Sciences, College of Basic Education, University of Sulaimani, Sulaimani, Iraq; e-mail: Abdullakarim2004@gmail.com

[2] Governorate of Sulaimani, Sulaimani, Iraq; e-mail: sazansafa10@gmail.com

[3] Department of Geology, College of Science, University of Sulaimani, Sulaimani, Iraq; e-mail: ezadin.mohamed@univsul.edu.iq

Abstract: The construction of dam is important for many reasons. Prior to construction, it is essential to assess the dam's base reservoir to identify any subsurface cavities. This study was conducted along nine electrical resistivity (ERT) profiles and eight induced polarization (IP) profiles, which are traditional ERT profiles, trending SW to NE direction in the reservoir part of the failed Chaq-Chaq dam NW of Sulaimaniyah city. The aim of this study was to delineate subsurface layers, underground features, determine the depth to bedrock, and investigate indications of the causes of collapse of the constructed Chaq-Chaq dam. The Res2Dinvx64 program used in the inversion method to obtain true 2D resistivity sections using a Schlumberger-Wenner array, which is highly sensitive to changes in resistivity both vertically and laterally. Based on the resistivity values, it was found that the area consists of three geological layers; the first layer consists of soil, while the second layer consists of rock fragments, the interface between them has disappeared because the first layer is thin, and the third layer is specified as consolidated and cohesive limestone of the Kometan Formation. The surface of the Kometan limestones is irregular due to weathering and faulting resulting from tectonic movements leading to the collapse of the area and later filled with sediments of recent deposition. The IP method was only used to distinguish clay and water. According to IP values, water is present in the subsurface of the study area. According to the ERT sections, a sinkhole with a depth range of (15 – 39 m) was encountered at the beginning of most of the profiles. The occurrence of subsurface sinkholes and cavities in the fractured limestone of the Kometan Formation, especially in the western part of the dam region, is considered to be a contributing factor to the collapse of the dam when it is filled with water and subjected to the water pressure.

Key words: electrical resistivity tomography, induced polarization, water dam collapse, Iraqi Kurdistan region

*corresponding author, e-mail: Abdullakarim2004@gmail.com

doi: 10.31577/congeo.2024.54.3.1

1. Introduction

Water is an important resource in everyday life and in the global economy. Its development has been driven primarily by a lack of water during the dry season. A dam is a structure built across a river with the intention of raising the water level to form a reservoir (*Energy education, 2021*). Reservoirs (the dam basin and the upstream side on which water is collected) are used to store water, particularly when there is a surplus. In addition, they are used for flood control, irrigation, power generation, navigation, urban and industrial supply, fish farming, and tourism. Dams have many benefits, such as stored water and supply water for irrigation. Dams prevent the occurrence of flooding by collecting excess water to prevent it from flowing downstream (*Abdelwahed, 2019*).

The destroyed Chaq-Chaq dam was one of the small core clay body dams that was constructed about 2 km northwest to Sulaimani city in Kurdistan region – Iraq. This dam was especially needed for flood control, irrigation, and navigation in the region. The dam collapsed on 4th of February, 2006. This dam is a zonal earth dam with a gravelly shell and a clay core in the middle. The Chaq-Chaq dam was created by engineers with limited expertise in dam design and construction. One of the most significant mistakes in the design, which has been acknowledged, was the choice to locate the spillway in the identical valley as the dam, rather than as a stand-alone structure. The spillway wall has been made vertical. When building embankment dams, it is not advised to compact the embankment close to the vertical wall because this will cause a weak link to form at the point where the wall and embankment meet (*FEMA, 2005*).

Since the 1920s, geophysical methods had been employed in dam site surveys and safety monitoring. The selection of specific geophysical methods depends on the exact target and the geological conditions encountered in the field (*Tsai and Lin, 2022*). *Saleh et al. (2010)* revealed that geophysical methods are often used in site investigation to determine depth to the basement and map the characteristics of the subsurface prior to excavation and construction. The use of multiple geophysical methods helps to obtain more accurate results.

Zhao et al. (2021) believed that dam failures were caused by cracks, uncontrolled water flow through the dam, water leaking, joint separation due to poor design and construction. These ground surface conditions and the

nature of the dam construction may cause dam to collapse. Overlooking subsurface elements such as underground cavities, sinkholes, faults, and joints can also lead to more serious problems that may result in dam collapse. Subsurface characteristics could impact both the surface and underground areas below the dam, including its body and structure. Consequently, a comprehensive assessment of these factors is necessary to prevent the complications witnessed in the dam area. Evidently, in the surrounding area of the dam, the underground fractured Kometan limestone has abundant cavities, voids, and sinkholes, supplying Sarchnar springs with fresh water throughout the year.

Loke (1999) suggested that the Wenner-Schlumberger array is moderately sensitive to both vertical and horizontal structures. *Dahlin and Zhou (2004)* expected that the most commonly used arrays in the 2D electrical imaging surveys are conventional arrays such as the Wenner, Schlumberger, or Dipole-Dipole arrays. *Capizzi et al. (2005)* mentioned electrical resistivity tomography as the most widely used method for detection of underground voids. A study conducted by *Othman et al. (2019)* had used 2D resistivity method to determine the suitability of the Mirakan site (Erbil Governorate, Kurdistan Region – Iraq) for dam construction to store and supply the people with fresh water especially in summer season. *Aziz (2005)* used 2D resistivity tomography for the first time for a hydrogeological study in Bazian Basin – west of Sulaimani city, northeastern Iraq. *Amin (2008)* applied electrical resistivity method to delineate aquifers and evaluate hydraulic parameters from surface resistivity measurements in Sharazoor Basin, northeastern Iraq.

Youssef et al. (2012a) used the integration of remote sensing and electrical resistivity methods to investigate sinkholes in Saudi Arabia, indicating unconsolidated material in the subsurface (karst phenomena). *Gardi et al. (2015)* applied two-dimensional electrical resistivity tomography (ERT) method to identify the nature of subsurface structures and assess their suitability for dam building to explore the dam site in Shaqlawa-Erbil Governorate, NE Iraq.

Shao et al. (2021) suggested that one geophysical method may provide ambiguity in interpretation of the subsurface layers, such as electrical resistivity, which is unable to distinguish between water and clay content, ERT with induced polarization (IP) are applied for this purpose. In this

article, IP data was employed as a supplementary technique to distinguish between water and clay layers in ERT. Conrad Schlumberger (*Schlumberger, 1920*) first convincingly described the IP response in his classic monograph 'Étude sur la prospection électrique du sous-sol' (*Baban et al., 2023*), applied combined ERT/IP methods and geoelectrical parameters to evaluate groundwater in Qularaisi NW Sulaimani City – Kurdistan region – Iraq.

Cardarelli et al. (2006) used electrical resistivity tomography to detect buried cavities in Rome. *Youssef et al. (2012b)* detected sinkholes using electrical resistivity tomography in Saudi Arabia. *Camarero and Moreira (2017)* applied electrical resistivity tomography on an earth dam. *Shanshal and Al-Heety (2020)* detected subsurface cavities using inverted synthetic models by 2D electrical resistivity tomography technique. *Moreira et al. (2022)* applied electrical resistivity tomography (ERT) in uranium mining earth dam.

The aims of this study are:

1. To investigate the suitability of the subsurface geological features, ground conditions and geological structures for the dam basin. The electrical resistivity method was applied for this purpose. The IP method was used to distinguish between water and clay only.
2. Determine the depth to bedrock, perform bedrock strength assessment.
3. Mapping of underground structures, fractures, voids and sinkholes and evaluation of the selected underground area for dam construction, "the dam basin".
4. Investigation of the causes of the collapse of the constructed Chaq-Chaq dam.

2. Location of the study area

The study area encompasses the Chaq-Chaq dam, situated approximately 2 km northwest of Sulaimaniyah city in the Kurdistan region of Iraq. The Chaq-Chaq dam basin is located in the Chaq-Chaq stream valley, which falls between the plunges of the Sulaimani anticline, the western side of the Sulaimani anticline lies on the site of the dam (study area), while the eastern Sulaimani anticline is located in the eastern part of the area due to the strike slip fault that cuts the Sulaimani structure (*Al-Hakari, 2011*).

The study area, comprising the reservoir basin, covers an estimated area of about 45,039 m^2 with a relatively flat topography showing slight undulations ranging from 768 to 771 metres, as illustrated in Fig. 1. This specific site was selected due to the lack of geophysical studies in the vicinity. A solitary previous geophysical study (seismic refraction tomography) conducted by *Baban et al. (2022)* is available, along with supplementary verification tools such as outcrop information, which significantly aids in data interpretation.

The governorate of Sulaimani is located in the Northeast of Iraq. According to *Al-Qayim, et al. (2019)*, the northern and eastern sections of Sulaimaniyah city have undulated landforms characterized by various stages of alluvial fan formation on the mountain fore-slopes. The low altitude section of the mountain pediment covers the middle part of the Sulaimaniyah

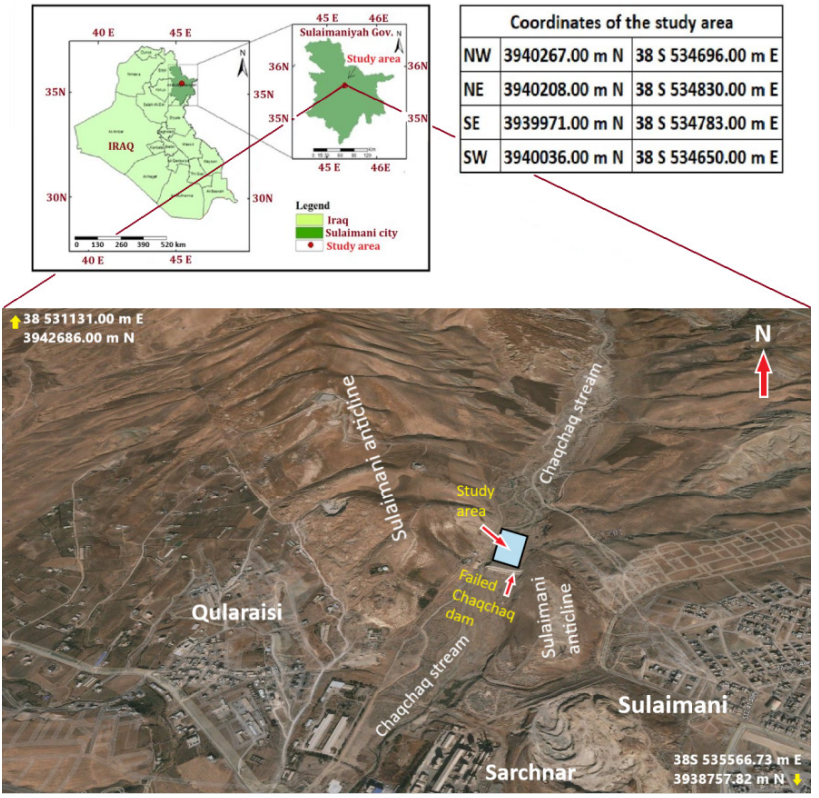

Coordinates of the study area		
NW	3940267.00 m N	38 S 534696.00 m E
NE	3940208.00 m N	38 S 534830.00 m E
SE	3939971.00 m N	38 S 534783.00 m E
SW	3940036.00 m N	38 S 534650.00 m E

Fig. 1. Location map of the study area (*Google Earth, 2022*).

city area. During the early phases of the city's development, expansion was limited to the east of the Chaq-Chaq valley and over a drainage network of low-order streams (orders two and three) (*Al-Qayim, et al., 2019*).

The outcrop of the Kometan Formation, alongside recent deposits comprising soil and rock fragments, was observed in the field. Within the Kometan Formation, predominantly composed of limestone, outcrops were visible on both the eastern and western perimeters of the study area, shaping the valley basin within. The thickness of recent deposits varied across the study area; in some locations, it measured less than 1m, while in others, it exceeded this depth. Notably, a layer of recent deposits was identified within specific coordinates, such as between longitude 534788.23 m E and latitude 3940115.19 m N and longitude 534685.81 m E and latitude 3940103.69 m N, as depicted in Fig. 2.

Fig. 2. Photo image shows the layer thickness and types of layers.

3. Geology and tectonic setting

3.1. Geology

The geological setting of Iraq allows such a quality profile with its sedimentary cover of 4 – 13 km thickness that overlies the Precambrian basement. Kometan Formation (Late Turonian – Early Campanian) was firstly described by *Dunnington (1958); Jassim and Goff (2006)*. Lithologically, it

consists of white-to-light-gray, hard, uniform and medium-bedded limestone and chalky limestone *Al-Qayim et al. (2012)*. The thickness of its composition reaches 100 – 120 m (*Karim et al., 2008*). This formation is cropping out in north, northeastern and northwestern parts on the limbs of Azmar-Goizha and Plunge of Piramagrun, and Sulaimani anticlines as well as in the western part of Sulaymaniyah city and this study area. Quaternary sediments based on field observations, there are two units of alluvium and some residual slope wash soil layers that exposed in Chaq-Chaq valley terraces which belonged to different periods of recent time.

The Zagros orogenic belt resulted from the collision of the Arabian and Eurasian Plates in the Cenozoic up to the present-day Fig. 3. The Zagros orogenic belt extends almost 2000 km across Iran and Iraq, through Syria and southeastern Turkey. The tectonic evolution of the Zagros can be sum-

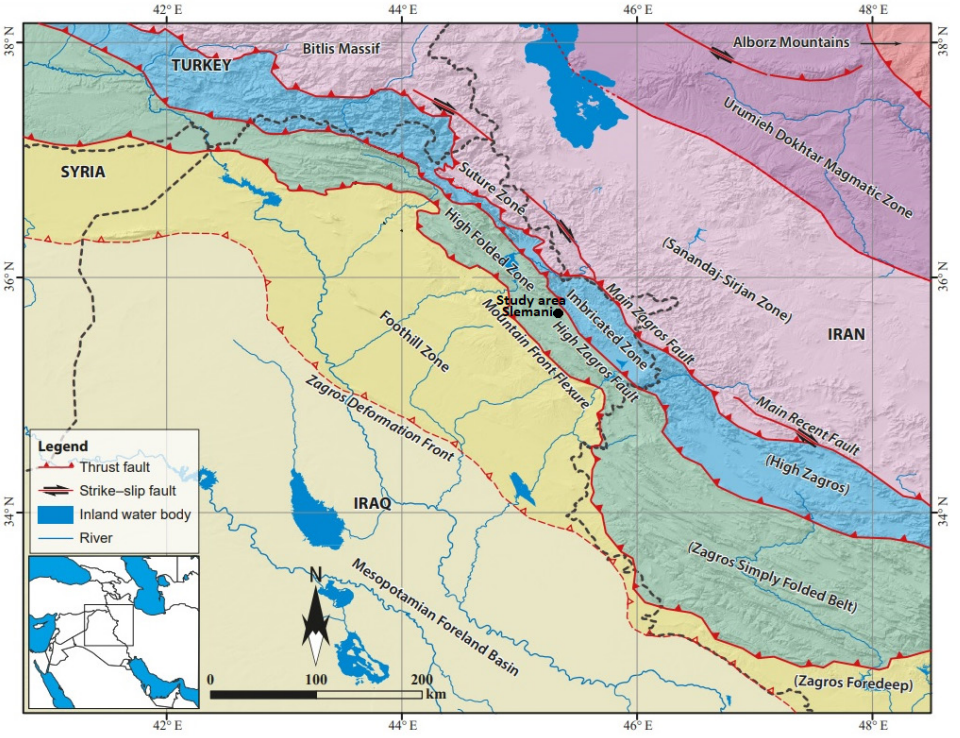

Fig. 3. Tectonic subdivisions of the NW segment of the Zagros Fold–Thrust Belt (modified by *Zebari et al., 2019*).

marized as a series of Late Proterozoic, Permian and Mesozoic rift events that were followed by closure of the ancient continental margin leading to continental collision in the Cenozoic (*Alavi, 2004*).

The Iraqi territory is the northeastern extension of the Arabian platform that surrounds the Arabian shield. Early workers subdivided the Arabian platform within the Iraqi territory into two major parts: a stable part to the southwest and an unstable part to the northeast *Dunnington (1958)*. These broad lines of definition were adapted latter by many workers, either under the same names or others, then further subdivided into smaller and smaller zones and subzones followed to describe the structural framework of Iraq (*Ditmar, 1971; Buday, 1980*).

3.2. Tectonic setting

Tectonically Iraq can be divided into two main tectonic units, Alpine Geosyncline and Nubian-Arabian Platform. The structure and structural development of Iraq is basically determined and strongly influenced by its position on the border between these two main Phanerozoic tectonic units of the Middle East (*Buday and Jassim, 1987; Baban, 2001*). The Apline Geosyncline unit is divided into External, Central, and Internal zones, each of them is divided into subzones.

Lawa et al. (2013) divided the Iraqi territories into four main tectonic zones, which are most widely used tectonic division these days. These Zones involve low folded thrust zone, high folded thrust zone, imbricated zone and suture zone. The boundary between these zones characterized by faults such as Zagros Mountain mentioned previously. Zagros Mountain front fault, high Zagros reverse fault and Zagros main suture fault. In addition to the transversal faults such as Sirwan-Khanaqin fault, lesser Zab Fault and great Zab fault.

Tectonically, the area involved in this study is located within the high folded zone, which lies in (Zakho-Sulaimani sub-zone) of north eastern part of Iraq and exactly within the Sulaimani-Sharazur Basin, on the Sulaimani anticline known as Harmetool Mountain according to *Bety (2013)*. According to *Al-Hakari (2011)* the Sulaimani anticline is around 2 km northwest of Sulaimani city that is falling in two directions: its northeastern plunge began before its southeastern plunge of the Piramagrun anticline, forming

Fig. 4. Geological structures around the Chaq-Chaq stream (modified from *Earth View, 2022*).

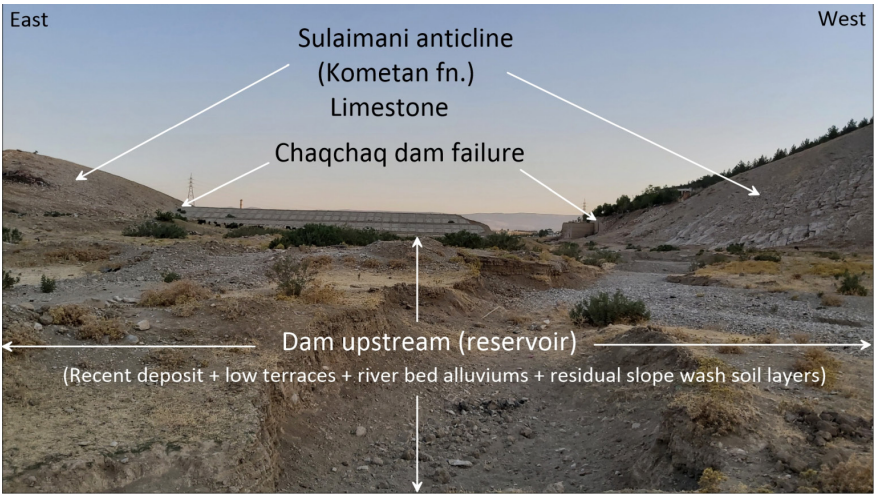

Fig. 5. Upstream (reservoir) side of the failed Chaq-Chaq dam (study area).

an echelon with it, and its southwestern plunge, which begins below Sulaimaniyah city as shown in Figs. 4 and 5. A small anticline, known as the Sherkuzha anticline, emerges as a minor structure extending in a northwest-southeast direction. This feature is situated adjacent to the Piramagrun, distinguished by a brief syncline. Towards the southeastern inclination, the fold bifurcates to create a surface exhibiting an anastomosing pattern, with

the Sherkuzha anticline set apart from the Sulaimani anticline by a slender syncline.

4. Hydrology and climate

Hydrologically, the study area's lowlands are confined to large valleys such as the Tanjero valley. Chaq-Chaq and Kanipan are the two important streams in the region, they flow from the north and northwest (*Bety, 2013*). The Tanjero stream, running approximately 13 km southwest of the city centre, originates from the merging of two streams near Kani-Goma village, situated about 7.5 km from the city centre. Serving as a primary water source for the Darbandikhan reservoir, located 50 km southwest of Sulaimaniyah city, the Tanjero Stream plays a crucial role in the region. Over time, the area has been shaped by alluvial and fluvial processes alongside periodic floods, influencing its development from the initial stages onwards.

A significant challenge in the study area was the absence of hydrological data, presenting a notable hurdle for the consultant. The lack of a hydrometric station in the basin led to insufficient data on crucial factors such as flow discharge, storms, sediments, water quality, and flood patterns – essential information vital to the study's comprehensive analysis.

The purpose of the climatology study is to recognize and estimate the values and perform frequency analysis of the most significant climate factors affecting the study area including precipitation, air temperature, wind, relative humidity, evaporation. Sulaimaniyah station which is located at latitude 35°33′ N and longitude 45°27′ E, at elevation 884.8 m. *Shahsavari (2012)* mentioned that 3-year drought period has occurred from 1978 to 1980 and there was drought period a 6-year period from 1997 through 2002 and another drought period was a 7-year period from 2005 through 2011 at Sulaimaniyah which is the nearest station to the dam site. Furthermore, some single drought years occur during the study period in 1973, 1975, 1980, 1983, 1989, 1990, 1999, 2005, 2008, 2017 and 2021 as shown in Fig. 6.

At Sulaimaniyah station, a total annual amount of precipitation recorded was approximately 1235.2mm since 2018. No precipitation was recorded in July from 2017 – 2021 because it was the warmest month in Sulaimaniyah, the total annual precipitation recorded in 2021 was approximately 291.9 mm, as shown in Fig. 7.

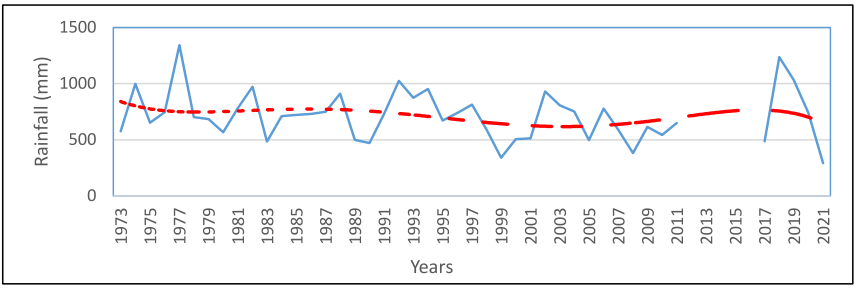

Fig. 6. The average of annual precipitation from years 1973 – 2021 collected and recorded at Sulaimaniyah station.

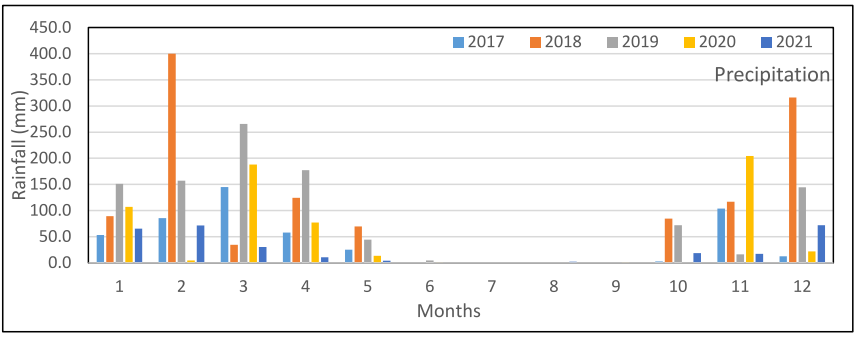

Fig. 7. The monthly average of precipitation from years 2017 – 2021 recorded at Sulaimaniyah station.

5. Methodology

5.1. Data acquisition

The fieldwork strategy involved segmenting the study area into nine Electrical Resistivity Tomography (ERT) and eight Induced Polarization (IP) profiles, oriented from southwest to northwest, to effectively detect bedrock layers. Situated in the northern region of the Chaq-Chaq dam, all profiles ran parallel to each other. Utilizing the ABEM Terrameter LS (*Guideline Geo AB, 2021*) from Guideline Geo, Sweden, a single-channel instrument, both ERT and IP methods were applied for data collection.

For the resistivity survey setup, a resistivity meter with four electrodes was employed, equipped with a multi-electrode survey system for 2D analy-

sis. The ABEM Terrameter LS instrument featured a total of 41 electrodes, connected through four cables spanning approximately 200 metres in total length, each with a takeout ranging between 10 and 11 metres.

The electrical resistivity survey commenced during the autumn season, initiating ERT profiling across the nine designated profiles extending from southwest to northeast. Distinct spacing intervals were observed between individual profiles, with precise recording of South and North coordinates for each line is documented in Table 1.

Table 1. Number of profiles, direction, and coordinates for electrical resistivity and induced polarization method.

No. of profiles	South coordinates		North coordinates	
	East	North	East	North
ERT-Tr-1	534783	3939971	534824	3940178
ERT-Tr-2	534766	3939981	534806	3940192
ERT-Tr-3	534746	3939992	534788	3940201
ERT-Tr-4	534729	3939998	534772	3940210
ERT-Tr-5	534712	3940008	534753	3940218
ERT-Tr-6	534694	3940014	534734	3940225
ERT-Tr-7	534674	3940024	534715	3940231
ERT-Tr-8	534665	3940028	534705	3940230
ERT-Tr-9	534650	3940036	534690	3940240

The pre-installed array types in this instrument consist of multiple Gradient, Dipole-Dipole, Wenner, Schlumberger, Pole-Dipole and Pole-Pole. All profiles have been acquired using the Wenner-Schlumberger protocol of 524 apparent resistivity data reading measurements for each (41) electrode profile. The electrical resistivity data acquisition layout was created at the beginning prior to the survey, as shown in Fig. 8.

A total of 41 electrodes were placed to perform the ERT profile, which were arranged in a straight line along the measurements. The electrode spacing was 5 m for all electrical resistance profiles as shown in Fig. 9, except for the first profile, which was 3 m. The total length of each profile was 200 m, except for the first profile (120 m). For each profile, 524 apparent resistivity data readings were recorded.

Four profiles (ERT-Tr-1, ERT-Tr-7, ERT-Tr-8 and ERT-Tr-9) were conducted during the autumn season in the Chaq-Chaq upstream (Reservoir)

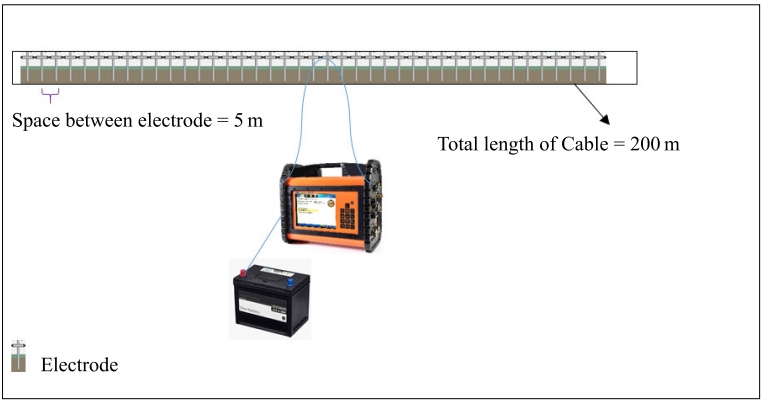

Fig 8. Electrical resistivity tomography data acquisition layout.

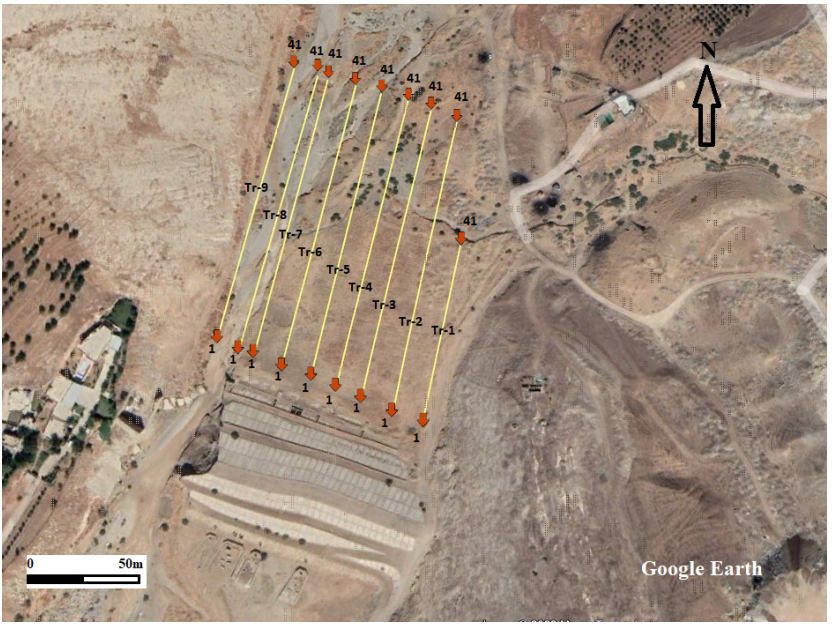

Fig. 9. Nine profiles for ERT method in study location (*Google Earth, 2022*).

of the dam, while other five profiles (ERT-Tr-2, ERT-Tr-3, ERT-Tr-4, ERT-Tr-5, and ERT-Tr-6) were executed during spring season as shown in Fig. 10.

Fig. 10. Shows the field work and the linear spread configuration of profile 9.

5.2. Data processing

The Res2Dinvx64 software was utilized in this study to create the flow chart (Fig. 11) that illustrates the steps of the Electrical Resistivity Tomography

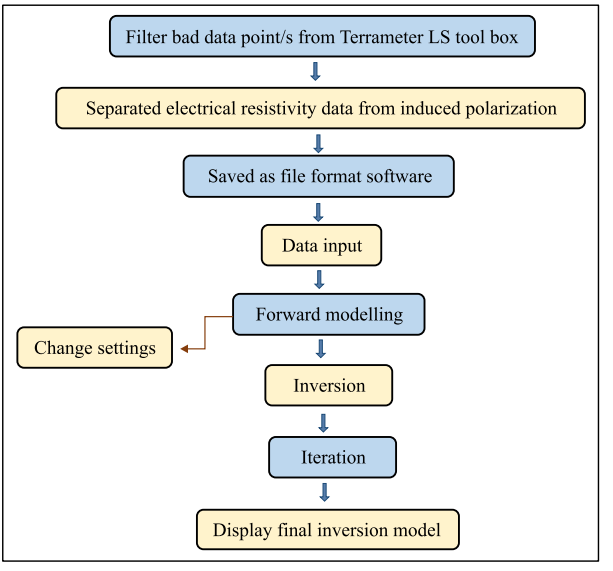

Fig. 11. Flow chart shows data processing for electrical resistivity tomography by Res2Dinvx64 software.

(ERT) process. The Tetrameter LS toolbox was used to sort and measure all recorded data for the generation of 2D ERT. The electrical resistivity data, excluding induced polarization, were saved in separate files. These data were then used as input to the Res2Dinvx64 software for forward modelling, using different settings applied for inversion by varying the number of iterations for all profiles. Finally, the final inversion model was prepared for interpretation and display. The main objective of the inversion algorithm was to find a subsurface resistivity model that closely matches the measured apparent resistivity data through theoretical (computed) response.

6. Interpretation of the results

Table 2 provides a summary of the RMSE and iteration number for all nine electrical resistivity tomography and induced polarizations. The values of %RMS below 5 are appropriately processed and represented. The interpretation results are presented in two figure parts, which include the following:

a) Inverse model resistivity section.
b) Inverse model chargeability section.

Table 2. The RMSE and iteration number of all nine electrical resistivity tomography and eight induced polarizations.

Profile	RMSE (%)	Iteration number	Profile	RMSE (%)	Iteration number
ERT-Tr-1	1.25	7	IP-Tr-1	1.2	7
ERT-Tr-2	4.4	7	IP-Tr-2	0.12	4
ERT-Tr-3	4.9	5	IP-Tr-3	–	–
ERT-Tr-4	3.5	7	IP-Tr-4	0.25	4
ERT-Tr-5	4.1	6	IP-Tr-5	0.14	7
ERT-Tr-6	5	7	IP-Tr-6	0.10	6
ERT-Tr-7	0.85	9	IP-Tr-7	1.3	7
ERT-Tr-8	1.96	7	IP-Tr-8	12.1	6
ERT-Tr-9	1.62	6	IP-Tr-9	3.6	6

ERT-Tr-1 profile

Figure 12 illustrates a 2D resistivity inverse section for the ERT-Tr-1 profile. Three horizontal layers are evident in this section. The interface between

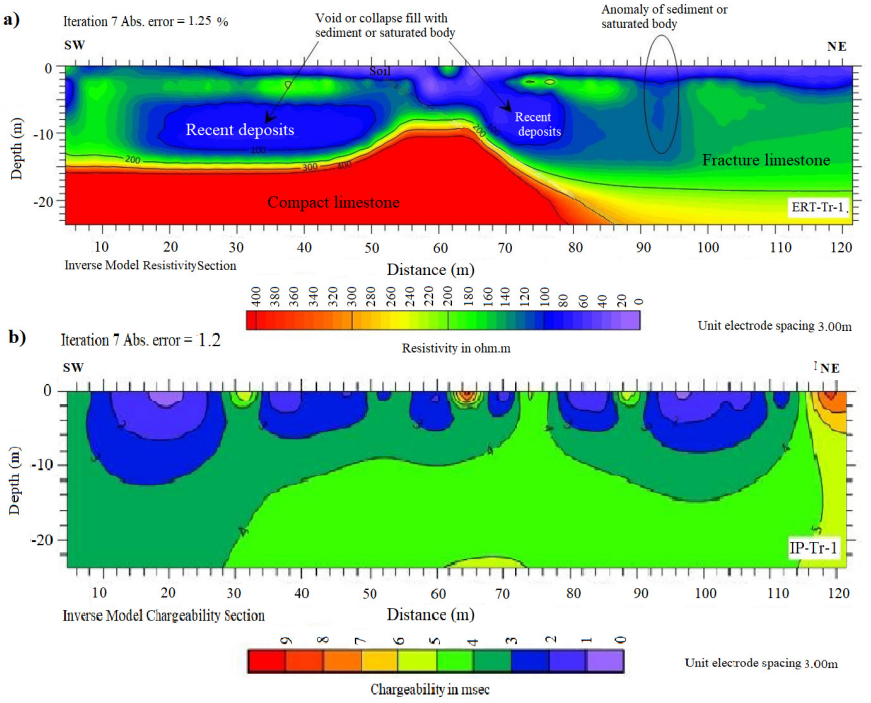

Fig. 12. Geoelectrical section from 2D inversion model result in ERT-IP-Tr-1 profile.

the first and second layer is invisible. The thickness of the first layer ranges from 0 – 2.5 m, which is the surficial layer in average, with resistivity values ranging from 0 – 50 Ω.m, corresponding to sediments or soil from recent deposits that cover the floor of the upstream of the dam reservoir. The second layer consists of rock fragments with thickness ranging from 1 to 12 m. The rock fragments are characterized by higher resistivity values than the first layer and range from 51 – 100 Ω.m. The top of third layer is located at depths ranging from 2 to 13 m and consists of fractured limestone with resistivity ranging from 101 to 399 Ω.m. At a distance of 0 – 80 m, the rocks have extremely high resistivity values equal to and greater than 400 Ω·m, indicating the presence of hard and compact limestone that appeared at a depth of 10 – 12 m.

There are many anomalies in the ERT section as shown in Fig. 12a, from the right side of the section at a distance of 68 – 78 m, another anomaly has appeared due to a collapse that has been filled by recent deposits or

may be a saturated body. Another anomaly represented on the left at a distance of 18 – 51 m relates to a sinkhole filled by recent deposits or may be a saturated body. The right side of the section at 92 – 96 m shows a narrow vertical collapse and infill by a recently deposited or possibly saturated body. Figure 12b shows a 2D IP section for the IP-Tr-1 profile. Depending on the IP values, the first and second layers consist of saturated recent deposits. This method removes the ambiguity between clay and water content. According to this method, the recent deposits are filled with water because they have a low electrical resistivity value and a low IP value, and they are in the range of 0 – 3 msec.

ERT-Tr-7 profile

The electrical resistivity tomography section for the ERT-Tr-7 profile is shown in Fig. 13a. The interface between first and second layers is invisible because the first layer is thin. The resistivity values for the first and second

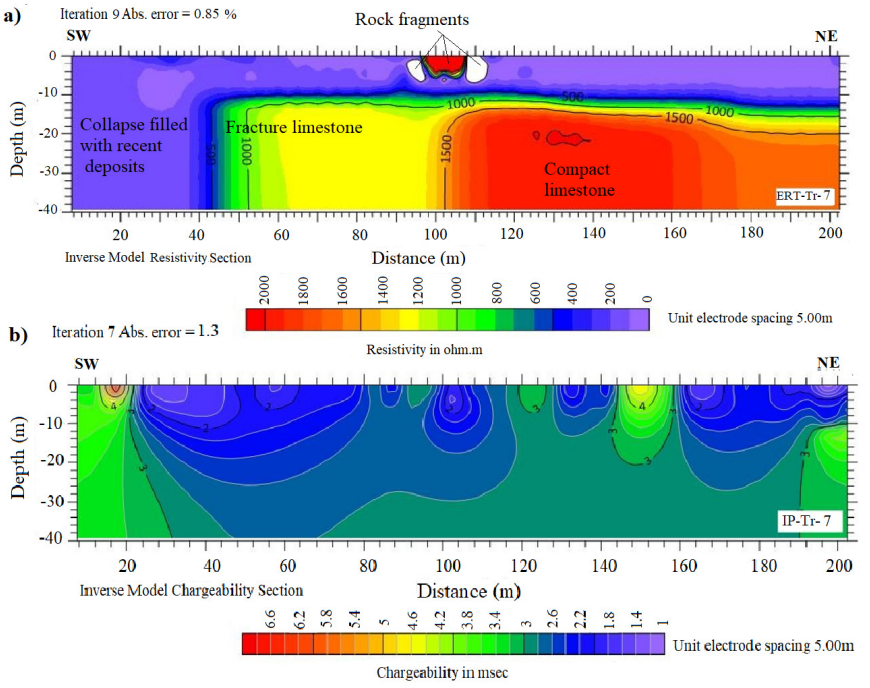

Fig. 13. Geoelectrical section from 2D inversion model result in ERT-IP-Tr-7 profile.

layers were 0 – 100 Ω.m, which corresponds to soil and rock fragments from recent deposits that cover the floor of the upstream of the dam reservoir. The interface between the second and third layers is clearly visible at a depth of 8 – 12 m ant at a distance of 39 – 41.5 m.

The third layer consists of two parts; the first is observed at the top of this layer and consists of fractured limestone with different resistivity values ranging from 201 – 1900 Ω.m. Below this part, hard and compact limestones with high resistivity values in the range of 1901 – 2100 Ω.m are evident at 17 – 20 m depth and at a distance of 112 – 160 m.

From distance 38 m, one reverse fault may be present. One deep collapse at distance ranging from 0 – 38 m is evident and may be generated due to this fault. This collapse was filled by sediments of recent deposition. Three small anomalies consisting of rock fragments of limestone, gravel or sand were observed in the centre near the surface between a distance of 93 – 113 m and are characterized by high resistivity values in the range of 2000 – 2100 Ω.m. One void was observed at distances ranging from 24 – 40 m and at distances ranging from 3 – 14 m. Figure 13b shows a 2D IP section for the IP-Tr-7 profile. The first and second layers consist of saturated recent deposits with IP values ranging from 1 – 2.8 ms. According to this method, recent deposits filled with water had a low electrical resistivity value and a low IP value.

ERT-Tr-8 profile

Figure 14a illustrates the electrical resistivity tomography section for ERT-Tr-8 profile. First layer mixed with second layer and interface between them disappeared because first layer is thin. The thickness of first layer and second layer together (recent deposits) ranges from 3 to 8 m, which is considered to be a soil with rock fragments with resistivity values ranging from 0 to 200 Ω.m. The depth of the third layer starts in the range of 4 – 9 m. The top of third layer consists of fractured limestone, whose resistivity value ranges from 201 – 1400 Ω.m. The bottom of third layer has a high resistivity value indicating a solid limestone in the range of 1401 – 1600 Ω.m. There may be one reverse fault at a depth of 4 m at a distance of approximately 78 – 80 m. One collapse observed at distance ranging from 0 to 73 m is filled by recent deposits and may have formed due to this fault. A single void is evident near the surface at a distance of 112 to 118 m.

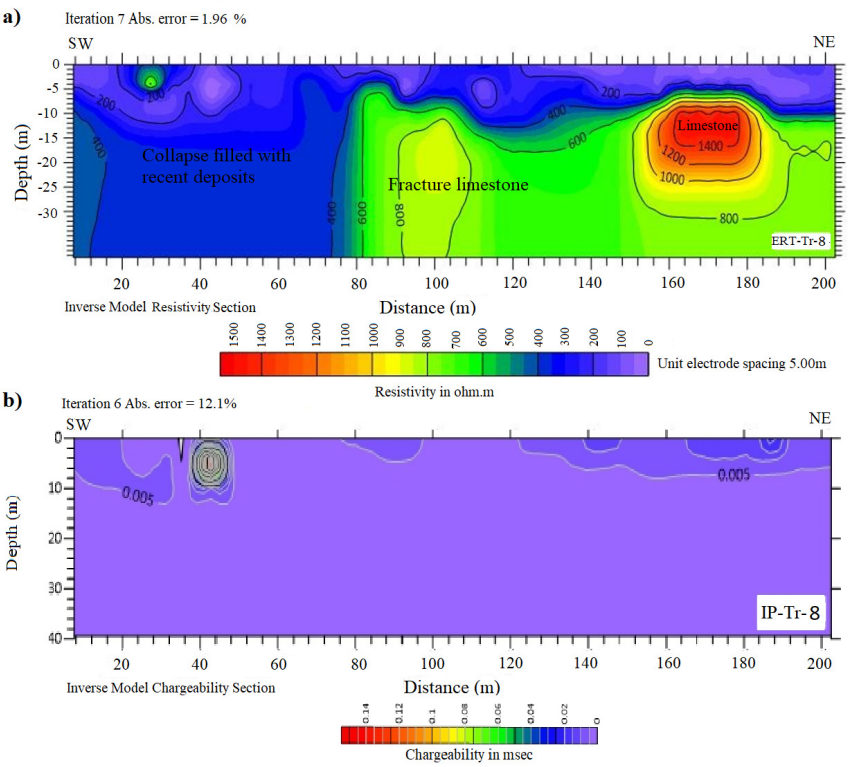

Fig. 14. Geoelectrical section from 2D inversion model result in ERT-IP-Tr-8 profile.

One small collapse is visible near surface at a distance of 0 to 50 m and is filled with sediments of recent deposition. A small green sphere shape appears near the surface at distances ranging from 14 to 32 m, with resistivity values ranging from 400 to 700 Ω.m, indicating a fractured limestone according to 2D IP section for IP-Tr-8 profile illustrated in Fig. 14b. The recent deposits, which consist of soil and rock fragments and as a result of having low IP value ranging from 0.0 to 0.02 ms, suggest the existence of water in the recent deposits. At the same time, water is present in the fracture at the top of the third layer due to the low IP value.

ERT-Tr-9 profile

The electrical resistivity tomography section for the ERT-Tr-9 profile is displayed in Fig. 15a. Recent deposits present and consist of soil and rock

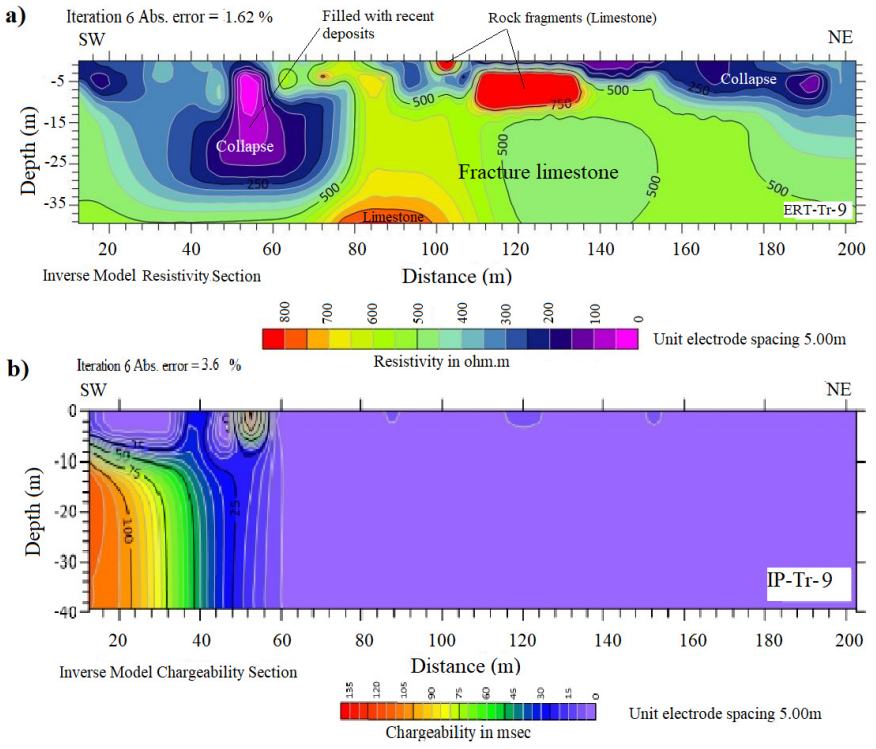

Fig. 15. Geoelectrical section from 2D inversion model result in ERT-IP-Tr-9 profile.

fragments having resistivity value ranges between 0 – 200 Ω.m. The top of the third layer is located at distance between 0 and 27 m, with resistivity values ranging from 201 to 750 Ω.m indicating fractured limestones. Hard and compact limestone with high resistivity values ranging from 751 – 850 Ω.m is found at a depth of 36 m.

In the middle of the section, the thickness of recent deposits decreased and a small elliptical-shaped anomaly (red colour) with a high resistivity value in the range of 751 – 850 Ω.m was observed at a distance of 108 – 139 m, indicating pieces of hard limestone. A single collapse is present between 10 and 78 m, which is filled with recent deposits. At a distance of 99 to 108 m near the surface in the middle of the section, one small hemispherical anomaly is visible, which has a high resistivity value and consists of pieces of limestone. Another collapse was observed on the right side at a

distance of approximately 135 – 194 m, which was filled by recent deposits. Based on the 2D IP section for the IP-Tr-9 profile that was displayed in Fig. 15b, water is present in this region, which has low ERT and IP values and ranges from 0.0 – 15 ms.

7. Discussion

Resistivity profiles showed a distinct three-layered profile with a high-resistivity layer at the base overlain by a middle layer and an uppermost layer with a low resistivity. The two upper layers are interpreted as recent deposits divided into two resistive layers that consisted of soil in the upper layer and rock fragments in the middle layer, which had a low resistivity value. The high resistivity layer in the bottom of the profiles was interpreted as rock that consisted of weathered limestone from the top and hard and compact limestone below.

Resistivity values vary based on profiles. In the case of the ERT-Tr-1 profile, a thin layer of soil covering the study area was reported with an average thickness ranging from 0 to 2.5 m, and the second layer consists of rock fragments ranging from 4 to 13 m in thickness and the interface between the two is invisible. In the case of the ERT-Tr-1 profile, the resistivity values for the overburden layer were 0 – 100 Ω.m, for the fractured limestone 101 – 399 Ω.m and for the compact limestone 400 Ω.m. For the ERT-Tr-7 profile, the resistivity value for the overburden layer was 0 – 100 Ω.m, for the fractured limestone the resistivity value ranged from 201 – 1900 Ω.m, and for the hard limestone the resistivity value ranged from 1901 – 2100 Ω.m. For ERT-Tr-8, the resistivity value of the overburden layer was 0 – 100 Ω.m, for fractured limestone the resistivity value ranged from 101 – 1400 Ω.m and for solid and compact limestone the resistivity value ranged from 1401 – 1600 Ω.m. And for ERT-Tr-9, the resistivity value of the profile for overburden layer was 0 – 200 Ω.m, for fractured limestone the resistivity value ranged from 201 – 750 Ω.m and for solid and compact limestone the resistivity value ranged from 751 – 850 Ω.m.

For all other profile sections, the interface between the first and second layers was invisible because the first layer was thin and calculated with the second layer, with the first and second layers having the same composition. The first and second layers consist of recent deposits and can be called over-

burden layer. For profiles ERT-Tr-2, ERT-Tr-3, ERT-Tr-4, ERT-Tr-5 and ERT-Tr-6, the overburden layer covered the bedrock of the dam reservoir floor (upstream) and its thickness ranged from 1 – 16 m on average and had resistivity values ranging from 0 – 100 Ω.m. The thickness value of the recent deposits varied from site to site at some locations, and this range was greater than this level due to present collapse or voids filled by the sediments of recent deposits. The upper part of the third layer started at a depth of 8 – 39 m and had varying resistivity values ranging from 101 to 1999 Ω.m, indicating fractured limestone that had eroded due to weathering and karstification. The bottom part of the third layer shows high resistivity values, which are higher than 2000 Ω.m and indicate hard limestone.

Several anomalous features were discovered throughout the ERT section, including collapses and voids filled with sediments of recent deposition. These anomalous structures lead to leakage and pose a risk to the safety and stability of the dam. This reservoir (dam basin-upstream) downstream of the dam contains a heavily fractured rocks, voids and sinkholes and water leakage via fractures in the sinkhole and voids floor and a significant amount of water entering the reservoir through fractures in the limestone bed, which is located in a highly fragmented karstic region. The ground water may be present in the study area depending on IP values, and surface water was present at depths of approximately 4 to 10 m, and at some locations at depths of 4 to 39 m due to existence of sinkholes and caverns and the water collected therein. Separation of clay (sediment) and water content is difficult with the ERT method alone because each has a low resistivity value, resulting in ambiguity in their resolution. For this purpose, by combining ERT with IP, the result was integrated to distinguish water and clay. According to *Johansson et al. (2007)*, clay has a low electrical resistivity value with a high IP value, whereas water has a low electrical resistivity value and an IP value.

The bedrock was determined to be approximately 15 – 39 m in depth; the resistivity of the limestone was highly dependent on t he degree of fracturing and the amount of water contained in the fractures. The ground water may be present in study area, especially at ERT-Tr-8 and ERT-Tr-9. The surface water was present at depths ranging from 4 to 10 m. Surface water is able to infiltrate the fractured rock and collect in the collapse, so it spring here and can depend on a limited period. This has been confirmed by a

hand-dug well near the study area approximately 40 m from the ERT-Tr-1 profile. This well was dug by hand to a depth of 10 m and water appeared at 4 m. The upper part of the third layer starts at a depth of approximately 7 – 15 m (fractured limestone) and the lower part of the third layer of bedrock (compact limestone) starts at a depth of 15 – 39 m.

Depending on previous geophysical work (*Baban et al., 2022*), the results indicated that the first and second layers are weak and fissured and subjected to sinkholes buried by recent sediments, whereas the third layer indicates the harder-to fracture rocks. Based on this work, a sinkhole/cavity appeared at the beginning of most of the profiles with depths ranging from 15 – 39 m. The presence of sinkhole was related to the layers filling with water during the winter rainy season, after which the water penetrated deeply, leading to the collapse of the layers and the formation of this sinkhole. The presence of this sinkhole in the western part can be considered as the cause of the collapse of the dam after the application of water pressure on the dam, and also the side of the dam was not connected to the rocks forming the shoulder of the dam.

8. Conclusions

In general, the dam area consists of three layers depending on the resistivity value, with the first layer consisting of soil, the second of rock fragments and the third of fractured limestone of the Kometan Formation. The presence of surface water in the recent deposits at depth ranges from 2.0 to 14 m. Depending on the resistivity values along profiles ERT-Tr-8 and ERT-Tr-9, the profile might indicate the presence of ground water in the fractured Kometan limestone. The resistivity of limestones is highly dependent on the degree of faulting and the amount of water contained in the fractures. The ERT sections presented in this study indicate the presence of sinkholes with depths ranging from 15 – 39 m at the beginning of most of the profiles.

The collapse of the dam can be attributed to the presence of subsurface sinkholes and cavities in the fractured limestone of the Cometan Formation, particularly in the western area of the dam. These geological features played a significant role in the failure of the dam when it was filled with water and subjected to the resulting water pressure.

Acknowledgements. We would like to thank the Groundwater Directorate, especially Mr. Abbas Ali Ahmed (the Director), Dr. Peshawa, Dr. Twana, and Mr. Baqi for providing us ABEM Terrameter LS instrument. We would also like to thank Jimmy Adcock (ABEM Product Manager), Robin Karlsson (ABEM Technician) and Harry Higgs (ABEM Application Engineer) for providing us with information about the ABEM instrument.

References

Abdelwahed B., 2019: A review on building progressive collapse, survey and discussion. Case Stud. Constr. Mater., **11**, e00264, doi: 10.1016/j.cscm.2019.e00264.

Alavi M., 2004: Regional stratigraphy of the Zagros Fold-Thrust Belt of Iran and its pro-foreland evolution. Am. J. Sci., **304**, 1, 1–20, doi: 10.2475/ajs.304.1.1.

Al-Hakari S. H. S., 2011: Geometric analysis and structural evolution of NW Sulaimani area, Kurdistan region, Iraq. PhD thesis, University of Sulaimani, 309 p.

Al-Qayim B. A., Al-Rawi A. M., Al-Bassam K. S., 2019: Facies modeling and sequence stratigraphy of an Eocene carbonate–phosphorite ramp: Damlouk member, Ratga Formation, Western Desert, Iraq. Iraqi Bull. Geol. Min., **15**, 1, 15–30.

Al-Qayim B., Omer A., Koyi H., 2012: Tectonostratigraphic overview of the Zagros Suture Zone, Kurdistan Region, Northeast Iraq. GeoArabia, **17**, 4, 109–156, doi: 10.2113/geoarabia1704109.

Amin A. K., 2008: Aquifer delineation and evaluation of hydraulic parameters from surfacial resistivity measurements in Sharazoor basin, North East Iraq. PhD Thesis (unpublished), University of Baghdad, college of Science, 181 p.

Aziz B. Q., 2005: Electrical Imaging: 2D Resistivity Tomography as a tool for groundwater studies at Mahmudia Village, West Sulaimani City, Iraqi Kurdistan Region. J. Zankoy Sulaimani, Part-A, **8**, 1, 7–16, doi: 10.17656/jzs.10131.

Baban E. N., 2001: Geophysical study of selected regional lines in the Western Desert of Iraq. PhD thesis (unpublished), University of Baghdad, Iraq.

Baban E. N., Amin A. K., Ahmed K. M., 2023: Combined geoelectrical tomography (ERT/IP) methods and geoelectricaly parameters to evaluate groundwater in Qularaisi area NW Sulaimani – Kurdistan Region-IRAQ. Iraqi Natl. J. Earth Sci., **23**, 1, 1–34, doi: 10.33899/earth.2023.135144.1024.

Baban E. N., Amin A. K. Mohammed S. S., 2022: Seismic refraction tomography and geotechnical parametersy to assess the Chaqchaq dam failure in NW Sulaimani City, Kurdistan Region, Iraq. Iraqi Natl. J. Earth Sci., **22**, 2, 121–139, doi: 10.33899/earth.2022.135251.1027.

Bety A. K. S., 2013: Urban geomorphology of Sulaimani City, using remote sensing and GIS techniques, Kurdistan Region, Iraq. PhD thesis (unpublished), Faculty of Science and Science Education, University of Sulaimani, 253 p.

Buday T., 1980: The Regional Geology of Iraq, Vol 1: Stratigraphy and Paleogeography. Publications of Geological Survey of Iraq, Baghdad, 445 p.

Buday T., Jassim S., 1987: The Regional Geology of Iraq: Tectonics, Magmatism, and Metamorphism. In: Kassab I. I., Abbas M. J. (Eds.): Geology of Iraq, Geologic

Survey, Baghdad, 445 p.

Camarero P. L., Moreira C. A., 2017: Geophysical investigation of earth dam using the electrical tomography resistivity technique. REM – Int. Eng. J., **70**, 1, 47–52, doi: 10.1590/0370-44672016700099.

Capizzi P., Cosentino P. L., Fiandaca G., Martorana R., Messina P., 2005: 2D GPR and geoelectrical modelling – tests on man-made tunnels and cavities. In: Near Surface 2005 – 11th European Meeting of Environmental and Engineering Geophysics (cp-13-00172), Palermo, Italy, 4–7 September 2005, doi: 10.3997/2214-4609-pdb.13.B036.

Cardarelli E., Di Filippo G., Tuccinardi E., 2006: Electrical resistivity tomography to detect buried cavities in Rome: a case study. Near Surf. Geophys., **4**, 6, 387–392, doi: 10.3997/1873-0604.2006012.

Dahlin T., Zhou B., 2004: A numerical comparison of 2D resistivity imaging with 10 electrode arrays. Geophys. Prospect., **52**, 5, 379–398, doi: 10.1111/j.1365-2478.2004.00423.x.

Ditmar V., 1971: Geological conditions and hydrocarbon prospect of the Republic of Iraq (Northern and Central part). Technoexport report, OEC Lib., Baghdad.

Dunnington H. V., 1958: Generation, migration, accumulation and dissipation of oil in northern Iraq: Middle East. In: Weeks G. L. (Ed.): Habitat. AAPG Spec. Publ., Tulsa, 1194–1251, doi: 10.1306/SV18350C49.

Earth View, 2022: Earth view-map 3D, https://wolfsys.net/earth-view-map-3d.

Energy education, 2021: website, https://energyeducation.ca/encyclopedia/Hydroelectric_dam.

FEMA, 2005: Technical Manual: Conduits through embankment dams. Federal Emergency Management Agency (FEMA P-484), accsessible at https://damtoolbox.org/images/f/f9/FEMA484.pdf.

Gardi S. Q. S., Al-Heety A. J. R., Mawlood R. Z., 2015: 2D electrical resistivity tomography for the investigation of the subsurface structures at the Shaqlawa proposed dam site at Erbil Governorate, NE Iraq. Int. J. Sci. Res., **4**, 5, 607–614, SUB153991.

Google Earth Pro, 2022: https://earth.google.com/web/@35.60519814,45.37444929,848.97739863a,16777.06932493d,35y,-0h,0t,0r.

Guideline Geo AB, 2021: ABEM Terrameter LS, user guide. Accessible at https://www.guidelinegeo.com/product/abem-terrameter-ls-2/.

Jassim S. Z., Goff J. C., 2006: Geology of Iraq, 1st Edition. Dolin, Prague and Moravian Museum, Brno, Czech Republic, 341 p.

Johansson B., Jones S., Dahlin T., Flyhammar P., 2007: Comparisons of 2D and 3D inverted resistivity data as well as of resistivity and IP surveys on a landfill. In: Near Surface 2007 – 13th EAGE European Meeting of Environmental and Engineering Geophysics (P42), Istanbul, Turkey, 3–5 September 2007, doi: 10.3997/2214-4609.20146658.

Karim K. H., Ismael K. M., Ameen B. M., 2008: Lithostratigraphic study of the contact between Kometan and Shiranish formations (Cretaceous), in Sulaimaniyah governorate, Kurdistan region, NE Iraq. Iraqi Bull. Geol. Min., **4**, 2, 15–27.

Lawa F. A., Koyi H., Ibrahim A., 2013: Tectono-stratigraphic evolution of the NW segment OF the Zagros fold-thrust belt, Kurdistan, NE Iraq. J. Pet. Geol., **36**, 1, 75–96, doi: 10.1111/jpg.12543.

Loke M. H., 1999: Electrical imaging surveys for environmental and engineering studies. A practical guide to 2-D and 3-D surveys. Accesed at http://www.geo.mtu.edu/~ctyoung/LOKENOTE.PDF.

Moreira C. A., Guireli Netto L., Camarero P. L., Bertuluci F. B., Hartwig M. E., Domingos R., 2022: Application of electrical resistivity tomography (ERT) in uranium mining earth dam. J. Geophys. Eng., **19**, 6, 1265–1279, doi: 10.1093/jge/gxac082.

Othman P. S., Bapeer G. B., Bakir H. B., 2019: Application of 2D resistivity method for dam site investigation in Mirakan area, Qushtapa district, Erbil, Iraqi Kurdistan Region. Iraqi Geol. J., **52**, 2, 70–77, doi: 10.46717/igj.52.2.5Ms-2019-12-28.

Saleh H., Idris K., Kankara A. I., 2010: Economic impact of dam construction, the challenge and solution to agricultural productivity in Nigeria: A Case Study of Tura Dam in Mashigi Village, Kankara L.G.A., Katsina State J. Agric. Vet. Sci., **2**, 1, 35–44.

Schlumberger C., 1920: Étude sur la prospection électrique du sous-sol (Study on underground electrical prospecting). Gauthier-Villars, Paris, 94 p. (in French).

Shahsavari M., 2012: General Directorate of Dams and Reservoirs (GDDR), Chaq-Chaq2 Dam Studies, Stage A-Feasibility Study. Unpublished Report, 1159.9/R6008, 409 p.

Shanshal Z. M., Al-Heety A., 2020: Analyzing sensitivity and resolution of some electrical resistivity configurations for detecting subsurface cavities using inverted synthetic models by 2D electrical resistivity tomography technique. Iraqi Natl. J. Earth Sci., **20**, 2, 64–85, doi: 10.33899/earth.2020.170370.

Shao P., Shang Y., Hasan M., Yi X., Meng H., 2021: Integration of ERT, IP, and SP methods in hard rock engineering. Appl. Sci., **11**, 22, 10752, doi: 10.3390/app112210752.

Tsai C.-C., Lin C.-H., 2022: Review and future perspective of geophysical methods applied in nearshore site characterization. J. Mar. Sci. Eng., **10**, 3, 344, doi: 10.3390/jmse10030344.

Youssef A. M., El-Kaliouby H. M., Zabramawi Y. A., 2012a: Integration of remote sensing and electrical resistivity methods in sinkhole investigation in Saudi Arabia. J. Appl. Geophys., **87**, 28–39, doi: 10.1016/j.jappgeo.2012.09.001.

Youssef A. M., El-Kaliouby H. M., Zabramawi Y. A., 2012b: Sinkhole detection using electrical resistivity tomography in Saudi Arabia. J. Geophys. Eng., **9**, 6, 655–663, doi: 10.1088/1742-2132/9/6/655.

Zebari M., Grützner C., Navabpour P., Ustaszewski K., 2019: Relative timing of uplift along the Zagros Mountain Front Flexure (Kurdistan Region of Iraq): Constrained by geomorphic indices and landscape evolution modeling. Solid Earth, **10**, 3, 663–682, doi: 10.5194/se-10-663-2019.

Zhao M., Liu P., Jiang L., Wang K., 2021: The influence of internal erosion in earthen dams on the potential difference response to applied voltage. Water, **13**, 23, 3387, doi: 10.3390/10.3390/w13233387.